

Elsevier Editorial System(tm) for Progress in Oceanography  
Manuscript Draft

Manuscript Number: PROOCE-D-13-00181R2

Title: How much do tides affect the circulation of the Mediterranean Sea? From local processes in the Strait of Gibraltar to basin-scale effects.

Article Type: Full Length Article

Keywords: Strait of Gibraltar; tidal flows; eddy fluxes; water mixing; deep water ventilation; Western Mediterranean Sea.

Corresponding Author: Ms. Cristina Naranjo,

Corresponding Author's Institution: University of Malaga-CEIMAR

First Author: Cristina Naranjo

Order of Authors: Cristina Naranjo; Jesus Garcia-Lafuente; Gianmaria Sannino; Jose Carlos Sanchez-Garrido

Abstract: The effects of tidal forcing on the exchange flow through the Strait of Gibraltar and the circulation in the near-field region are revisited with a regional numerical model. Also a basin-scale model run is conducted in a first attempt to assess the impact of these local processes on the Western Mediterranean thermohaline circulation. In the Strait of Gibraltar, tides are found to (1) increase the exchange flow volume transport, (2) modify the hydrological properties of Atlantic inflowing waters through the enhancement of mixing, and (3) facilitate the drainage of Mediterranean deep water. In the far-field, the model reveals that these local processes can favor deep convection in the Gulf of Lion. Some thoughts are provided offering possible explanations.

1 How much do tides affect the circulation of the Mediterranean Sea?

2  
3 From local processes in the Strait of Gibraltar to basin-scale effects.  
4  
5  
6  
7  
8  
9

10 C. Naranjo<sup>a</sup>, J. Garcia-Lafuente<sup>a</sup>, G. Sannino<sup>b</sup>, J.C. Sanchez-Garrido<sup>a</sup>  
11  
12  
13  
14  
15

16 (a) Physical Oceanography Group, University of Málaga-CEIMAR, Málaga, Spain  
17

18 (b) ENEA, Ocean Modelling Unit, via Anguillarese 301, 00123, Rome, Italy  
19  
20  
21  
22  
23  
24  
25  
26  
27

28 Corresponding author address:  
29

30 Cristina Naranjo  
31

32 Grupo Oceanografía Física  
33  
34

35 ETSI Telecomunicación, Universidad de Málaga  
36  
37

38 Campus de Teatinos s/n  
39

40 29071 Málaga  
41

42 tel +34952132849  
43  
44

45 e-mail: [cnaranjo@ctima.uma.es](mailto:cnaranjo@ctima.uma.es)  
46  
47  
48  
49  
50  
51  
52  
53  
54  
55  
56  
57  
58  
59  
60  
61  
62  
63  
64  
65

**Abstract:**

The effects of tidal forcing on the exchange flow through the Strait of Gibraltar and the circulation in the near-field region are revisited with a regional numerical model. Also a basin-scale model run is conducted in a first attempt to assess the impact of these local processes on the Western Mediterranean thermohaline circulation. In the Strait of Gibraltar, tides are found to (1) increase the exchange flow volume transport, (2) modify the hydrological properties of Atlantic inflowing waters through the enhancement of mixing, and (3) facilitate the drainage of Mediterranean deep water. In the far-field, the model reveals that these local processes can favor deep convection in the Gulf of Lion. Some thoughts are provided offering possible explanations.

**Keywords:** Strait of Gibraltar, tidal flows, eddy fluxes, water mixing, deep water ventilation, Western Mediterranean Sea.

1  
2  
3  
4  
5  
6  
7  
8  
9  
10  
11  
12  
13  
14  
15  
16  
17  
18  
19  
20  
21  
22  
23  
24  
25  
26  
27  
28  
29  
30  
31  
32  
33  
34  
35  
36  
37  
38  
39  
40  
41  
42  
43  
44  
45  
46  
47  
48  
49  
50  
51  
52  
53  
54  
55  
56  
57  
58  
59  
60  
61  
62  
63  
64  
65

## 1 1. Introduction

2 The baroclinic exchange through the Strait of Gibraltar (SoG hereinafter) is  
3 forced by the buoyancy losses in the Mediterranean Sea (MS). They give rise to  
4 the characteristic anti-estuarine thermohaline circulation of the MS that starts at  
5 the SoG with the surface Atlantic Jet and ends at the same location with the  
6 deep outflow of Mediterranean waters. The average properties of the latter are  
7 basically determined by the buoyancy losses and the constraining topography  
8 of the SoG (Figure 1), which drives the intervening flows to the hydraulic limit  
9 and to a situation of maximal exchange (Armi and Farmer, 1985, 1986; Farmer  
10 and Armi 1988). Within this theoretical frame, Bryden and Kinder (1991)  
11 resolved the steady, two-layer maximal exchange problem for a simple but yet  
12 realistic geometry of the SoG by imposing the mean net evaporation over the  
13 MS as the proper reservoir condition. Despite ignoring relevant driving forces,  
14 the approach gives realistic predictions of the exchange.

15 The exchange involves different time-scales (Garcia-Lafuente et al., 2000, 2002  
16 a, b) and the forces ignored in the previous models, essentially tidal forces and  
17 meteorologically-driven pressure gradients should be included to obtain more  
18 accurate predictions. It is especially the case for the former that prevail over any  
19 other. Theoretical (Farmer and Armi, 1986; Helfrich, 1995), laboratory (Helfrich,  
20 1995), numerical (Wang, 1993; Sannino et al., 2004) and observational (Bryden  
21 et al., 1994, Vargas et al., 2006) studies show that tides increase the long-term  
22 exchange flow by means of eddy-fluxes. The easiest way to visualize this  
23 process is by decomposing the velocity and the layer thickness in slowly varying  
24 (overbar) and fluctuating (primed) components according to  $u = \bar{u} + u'$ ,  $h = \bar{h} +$   
25  $h'$  (in practice, the decomposition is achieved by applying a suitable filter). The

1  
2  
3  
4  
5  
6  
7  
8  
9  
10  
11  
12  
13  
14  
15  
16  
17  
18  
19  
20  
21  
22  
23  
24  
25  
26  
27  
28  
29  
30  
31  
32  
33  
34  
35  
36  
37  
38  
39  
40  
41  
42  
43  
44  
45  
46  
47  
48  
49  
50  
51  
52  
53  
54  
55  
56  
57  
58  
59  
60  
61  
62  
63  
64  
65

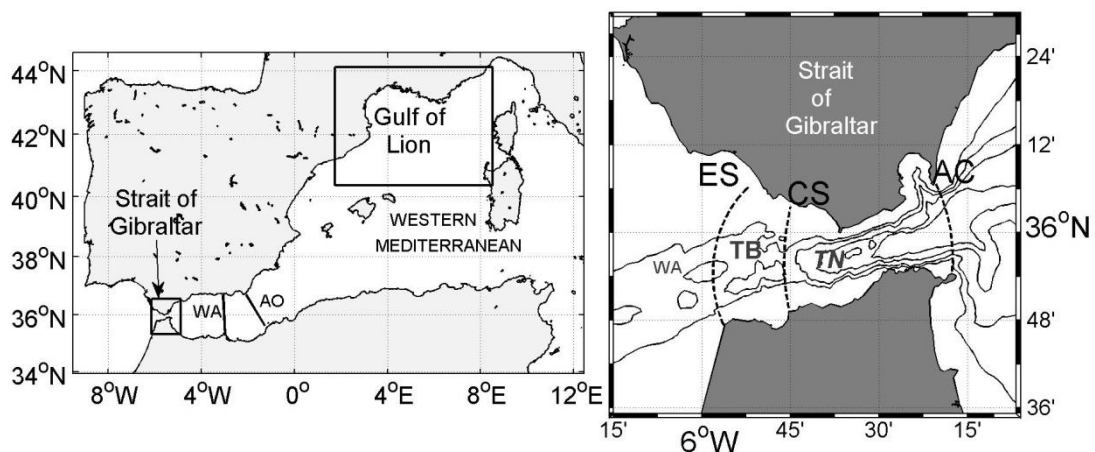
slow-varying flow, often called long-term flow, is defined as the exchange resulting from the time-average of the flow over a time window considerably longer than the tidal scale and is obtained as

$$\bar{q}_i = W(\bar{u}_i \bar{h}_i + \overline{u'_i h'_i}) \quad [1]$$

The first term of the right hand side is the quasi-steady contribution due to the mean fields whereas the second term is the eddy fluxes. Here  $W$  is a representative width and  $i=1,2$  indicates the Atlantic and Mediterranean layers. According to the observational analysis by Bryden et al. (1994), eddy-fluxes may account for up to 40% of the estimated long term flow. Subsequent experimental studies show that they depend on the location of the cross-section where they are computed (Garcia-Lafuente et al., 2000; Baschek et al., 2001; Sanchez Román et al., 2009), a result also reported in the numerical study by Sannino et al. (2004). Eddy fluxes show a clear dependence on the fortnightly tidal cycle (Vargas et al., 2006). The total flow, however, is less sensitive to the fortnightly tide since the enhanced mixing driven by strong currents during spring tides diminishes the quasi steady term in [1] and counterbalances the increased eddy-flux (Bryden et al., 1994; Vargas et al., 2006). This result agrees with the findings of Helfrich (1995) who shows that the exchange increases with the frequency and the strength of the barotropic fluctuations.

While the effect of tides on the volume transport is relatively well known, other processes are not. Tidally-induced mixing in the Camarinal sill area (CS hereinafter, Figure 1) is remarkably pronounced across the internal hydraulic jump at the western flank of the sill, and grows particularly vigorously when the shear between Atlantic and Mediterranean layer is enhanced by tidal flows. This leads to flow instability and turbulence as revealed by the observation of Kelvin-

1  
2  
3  
4  
5  
6  
7  
8  
9  
10  
11  
12  
13  
14  
15  
16  
17  
18  
19  
20  
21  
22  
23  
24  
25  
26  
27  
28  
29  
30  
31  
32  
33  
34  
35  
36  
37  
38  
39  
40  
41  
42  
43  
44  
45  
46  
47  
48  
49  
50  
51 Helmholtz billows and energy dissipation rates as large as  $10^{-2} \text{ Wkg}^{-1}$  (Wesson  
52 and Gregg, 1994), which are among the greatest ever recorded in the ocean.  
53 Sanchez-Garrido et al. (2011) show that the flow instabilities keep occurring in  
54 additional hydraulic transitions downstream of smaller-scale topographic  
55 features located in the Tangier Basin (Fig. 1), which enlarges the mixing area to  
56 the west. As a result, this basin is a remarkable source of Atlantic-  
57 Mediterranean mixed water that can be advected in either direction (Garcia  
58 Lafuente et al., 2013). Furthermore, tides are the origin of propagating internal  
59 bores and large amplitude nonlinear internal waves (Farmer and Armi, 1988;  
60 Vazquez et al., 2008; Sanchez-Garrido et al., 2013) with clear potential to  
61 increase mixing elsewhere in the SoG (Garcia-Lafuente et al., 2013). Whatever  
62 the specific process involved, mixing is so strong that it invalidates the simple  
63 description of the exchange in terms of two layers and requires the inclusion of  
64 a third interface mixing layer, which participates actively in the dynamic of the  
65 exchange (Bray et al. 1995; Sannino et al. 2007).



1  
2  
3  
4  
5  
6  
7  
8  
9  
10  
11  
12  
13  
14  
15  
16  
17  
18  
19  
20  
21  
22  
23  
24  
25  
26  
27  
28  
29  
30  
31  
32  
33  
34  
35  
36  
37  
38  
39  
40  
41  
42  
43  
44  
45  
46  
47  
48  
49  
50  
51  
52  
53  
54  
55  
56  
57  
58  
59  
60  
61  
62  
63  
64  
65

67 Figure 1. Left panel shows the Western Mediterranean Sea. The upper rectangle  
68 indicates the volume control in the Gulf of Lion used to compute the results of  
69 section 6. WA in the Alborán Basin indicates the Western Alborán section mentioned  
70 in the text, and AO indicates the Almería-Orán front. The lower small rectangle  
71 encloses the Strait of Gibraltar (SoG), which is zoomed on in the right panel. In this  
72 panel, ES, CS and AC indicate Espartel Sill, Camarinal Sill and Algeciras-Ceuta  
73 sections, respectively, which are used for doing computations. MB and TN represent  
74 Majuan Bank and Tarifa Narrows respectively. TB is the Tangier Basin that extends  
75 from CS to ES. Isobaths every 200m are shown from the surface to 1000m.

76  
77 The physical and biological consequences of this mixing in the nearby Alborán  
78 Sea basin and further east in the MS are poorly addressed and are awaiting for  
79 more in depth studies. According to several authors (Macías et al., 2007, 2008;  
80 Vazquez Escobar et al., 2009; Garcia-Lafuente et al., 2011, 2013) and as  
81 mentioned previously, a considerable volume of the biologically enriched waters  
82 in the area of strong mixing in CS is advected eastward, and eventually helps  
83 fertilize the Alborán Sea. In his paleoclimate study of the MS, Mikolajewicz  
84 (2011) found that the numerically modeled sea surface temperature in the  
85 Alborán Sea was greater than the observed climatology. He attributed this  
86 mismatch to the absence of tidal forcing in his model, which reduces the vertical  
87 turbulent fluxes of heat and salt. The result is a slightly warmer and more  
88 buoyant inflowing Atlantic surface water when tides are not included. The effect  
89 might be far-reaching taking into account that this inflow will be finally  
90 transformed into intermediate and/or deep Mediterranean water.

91 Another relevant issue for the MS circulation is the renovation of deep  
92 Mediterranean waters and the ventilation of the bottom layer. Western  
93 Mediterranean Deep Water (WMDW), which is formed in the Northwestern MS  
94 and spreads later over the Western Mediterranean basin, resides well below the  
95 main sill of Camarinal and must be uplifted above the sill depth in order to leave

1  
2  
3  
4  
5  
6  
7  
8  
9  
10  
11  
12  
13  
14  
15  
16  
17  
18  
19  
20  
21  
22  
23  
24  
25  
26  
27  
28  
29  
30  
31  
32  
33  
34  
35  
36  
37  
38  
39  
40  
41  
42  
43  
44  
45  
46  
47  
48  
49  
50  
51  
52  
53  
54  
55  
56  
57  
58  
59  
60  
61  
62  
63  
64  
65

96 the MS. The required energy would be supplied by the spatial acceleration that  
97 the flow undergoes as it approaches the SoG (Bernoulli suction), a topic which  
98 has been addressed in different studies (Stommel et al, 1973; Bryden and  
99 Stommel, 1982; Whitehead, 1985; Garcia-Lafuente et al., 2007, 2009; Naranjo  
100 et al, 2012). The remarkable intensity of tidal currents in the SoG is a relevant  
101 energy source for the aspiration of deep water that has not been mentioned in  
102 the literature except for the paper by Kinder and Bryden (1990). These authors  
103 detected traces of WMDW in the ocean side of the sill at the end of the west-  
104 going phase of some tidal cycles in spring tides, and speculated about the  
105 possibility that WMDW were routinely uplifted by tides. The authors could not be  
106 more conclusive and left the issue open for further research.

107 The present work addresses these topics with the help of two numerical models  
108 that have been run with and without tidal forcing in order to compare their  
109 outputs and thus assess the influence of tides on several hydrodynamic  
110 relevant features. The work is organized as follows. Section 2 describes the  
111 most relevant aspects of the numerical models already used in previous  
112 studies, which the readers are referred to for details. Section 3 revisits the  
113 relevant issue of the tidally-forced eddy fluxes in the SoG in the light of the new  
114 results provided by the models. Section 4 addresses the changes that tidally-  
115 induced mixing cause in the Atlantic inflow in the Alborán Sea and further east.  
116 Section 5 analyses the influence that tides could possibly have on the  
117 ventilation of WMDW near the SoG due to an enhanced Bernoulli suction. All  
118 these topics are of rather local or regional nature. In contrast, section 6  
119 addresses the far-field influence of tides by analyzing hindcast events of

120 WMDW formation during the decade of 1960. Section 7 summarizes the  
121 findings and conclusions of the study.

122

## 123 **2. Numerical Models**

124 The results of two numerical models based on the Massachusetts Institute of  
125 Technology general circulation model (MITgcm; Marshall et al. 1997a, b) source  
126 code have been used in this study.

127 The first model (RSGM, hereinafter) is sub-basin scale and it is exhaustively  
128 described in detail by Sanchez-Garrido et al. (2013). Just a brief summary is  
129 given here. The model uses the free-surface and hydrostatic configuration of  
130 the MITgcm and its domain covers the Gulf of Cádiz and the Alborán Sea. It is  
131 horizontally discretized with a curvilinear grid of variable spatial resolution. In  
132 order to better reproduce the mixing processes and the vorticity field in the SoG,  
133 the maximum resolution is achieved in the strait with a horizontal mesh size of  
134 around 300-500 m for both  $\Delta x$  and  $\Delta y$ , which gradually increases to some  
135 kilometers towards the east and west open boundaries. In the vertical the model  
136 has 46 unevenly distributed z-levels, with minimum cell thickness at the surface  
137 ( $\Delta z=5$  m). Vertical eddy viscosity and diffusivity coefficients are calculated  
138 according to the parameterization of Pacanowski and Philander (1981),  
139 whereas the turbulence closure scheme by Leith (1968) is chosen for the  
140 horizontal viscosity. The model is driven at the lateral open boundaries by the  
141 tracer and velocity fields provided by the Mediterranean forecast model (Oddo  
142 et al. 2009), whereas tides are introduced by forcing the model laterally with the  
143 tidal velocities produced by the barotropic tidal model of Carrere and Lyard

1  
2  
3  
4  
5  
6  
7  
8  
9  
10  
11  
12  
13  
14  
15  
16  
17  
18  
19  
20  
21  
22  
23  
24  
25  
26  
27  
28  
29  
30  
31  
32  
33  
34  
35  
36  
37  
38  
39  
40  
41  
42  
43  
44  
45  
46  
47  
48  
49  
50  
51  
52  
53  
54  
55  
56  
57  
58  
59  
60  
61  
62  
63  
64  
65

144 (2003). The model was run for a two-year spin-up period after which it produces  
145 realistic outputs.

146 The second model (GMSM, hereinafter) covers the whole MS, a brief overview  
147 is given here. Its grid is non-uniform, curvilinear orthogonal as well, with  
148 maximum horizontal resolution of about  $1/200^\circ \times 1/200^\circ$  (456 m) in the SoG.  
149 Eastwards and westwards of the SoG the resolution diminishes progressively  
150 until it reaches a grid size of  $1/16^\circ \times 1/16^\circ$  (5.7 km) in the rest of the domain. To  
151 resolve the dynamics of the different water masses in the MS adequately, 73  
152 unevenly spaced vertical z-levels were used, whose thickness range from 3 m  
153 at the surface to 300 m at the ocean bottom. The model is forced at the surface  
154 by the wind stress and the heat and fresh water fluxes derived from the  
155 dynamical downscaling of ECMWF ERA40 reanalysis performed with the  
156 regional atmospheric model RegCM (Artale et al. 2009). A surface relaxation to  
157 climatological temperature (5 days) and salinity (30 days) are also applied.  
158 Tides are incorporated in the model and tidal forcing includes both the tide  
159 generating potential as a body force in the momentum equations, and the lateral  
160 boundary condition in the open Atlantic boundary, which is impose in the same  
161 way as in the RSGM model.

162 Both models have been run with and without tidal forcing in order to assess the  
163 local, regional and far reaching effects of the tides. The characteristics of RSGM  
164 model make it more suitable for addressing local and regional issues as it  
165 produces hourly values compared to daily-means in GMSM; its outputs are  
166 used throughout sections 3 and 4. Although the simulation run covered the  
167 years 2010-2011, only the period from September to December 2011 has been  
168 used in this study. The period has been intentionally chosen because it

169 coincides with the period analyzed in Sanchez-Garrido et al. (2013) and  
170 Sammartino et al. (2014), during which a comprehensive model validation was  
171 carried out. The GSM model is used to address the question of how tides in  
172 the SoG could possibly affect relevant physical processes in the MS far away  
173 from the very strait, namely the deep water formation processes in the Gulf of  
174 Lion. This study makes use of the 1958-1968 hindcast in sections 5 and 6.

175

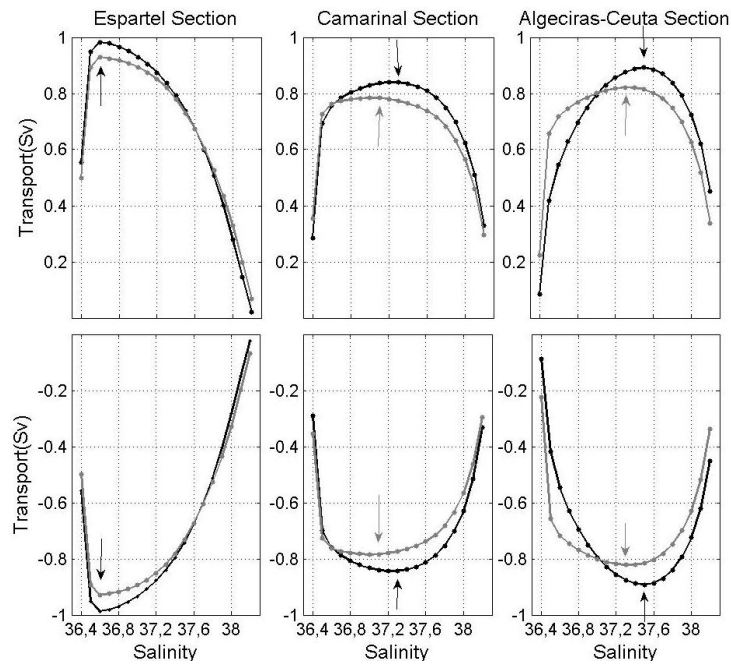
### 176 **3. Tides increase the long-term exchange flows**

177 This section revisits the issue of how tide-induced eddy-fluxes increase the  
178 exchanged flows, with the help of the RGSM model, which has proven to be  
179 more accurate than the one presented by Sannino et al. 2004 (see model  
180 comparison in Sannino et al., 2014). Following Garcia-Lafuente et al.(2000) and  
181 Baschek et al.(2001) the volume transport through a given cross-section is  
182 calculated by taking as the interface between Atlantic and Mediterranean waters  
183 the isohaline that maximizes the transport. A fresher isohaline would ascribe  
184 eastward-flowing Atlantic water to the Mediterranean layer, thus diminishing  
185 both the estimated inflow and the outflow. The same would occur if a saltier  
186 isohaline were selected, since westward-flowing Mediterranean water would be  
187 ascribed to the Atlantic layer. Figure 2 shows that this isohaline can always be  
188 found, although its specific value changes with the location. It also changes in  
189 the tidal and non-tidal runs at the same location. Table 1 shows the computed  
190 volume transport at CS section and at the two boundaries of the SoG, namely  
191 Espartel (ES, see Figure 1) and Algeciras-Ceuta (AC) sections, along with the  
192 isohaline that maximizes the exchange in both runs.

1  
2  
3  
4  
5  
6  
7  
8  
9  
10  
11  
12  
13  
14  
15  
16  
17  
18  
19  
20  
21  
22  
23  
24  
25  
26  
27  
28  
29  
30  
31  
32  
33  
34  
193 Focusing on section CS, the maximum exchange is achieved for isohalines 37.3  
194 and 37.1 for the tidal and non-tidal runs, respectively, and the corresponding  
195 transports are 0.84Sv and 0.79Sv, respectively, 6% higher in the tidal run. At  
196 ES, the isohaline that maximizes the flow is 36.6 (Fig. 2, Table 1) in both runs,  
197 an expected lower salinity than at CS. The transport at ES in the two  
198 experiments is larger than at CS, with the tidal run still giving a ~6% greater  
199 value (0.98 Sv versus 0.93 Sv). The lower salinity of the isohaline used as  
200 interface and the larger flow at ES compared with CS section are attributable to  
201 the entrainment of AW by the swift Mediterranean undercurrent in the western  
202 part of the SoG (Garcia-Lafuente et al. 2011). Likewise, the entrainment of MW  
203 by the overlying Atlantic jet leads to a more saline interface (around 37.4) and  
204 greater flows through AC section than at CS. The tidal run keeps on providing  
205 greater transports than the non-tidal run also in this section (0.89 Sv against  
206 0.82 Sv, ~8% increase)

35  
36  
37  
38  
39  
40  
41  
42  
43  
44  
45  
46  
47  
48  
49  
50  
51  
52  
53  
54  
55  
56  
57  
58  
59  
60  
61  
62  
63  
64  
65  
207 It is interesting and illustrative to explore the decomposition of transport in terms  
208 of the slowly-varying and eddy-fluxes contributions shown in Equation [1]. Table  
209 1 indicates that the contribution of eddy-fluxes to the total flow at CS is very  
210 large (0.32Sv or 38%), whereas they decrease dramatically to 3% and 1.4% at  
211 the bounding sections of ES and AC respectively. These results agree with the  
212 findings of Bryden et al. (1994) who reported eddy-fluxes as high as 50% at CS,  
213 and with Vargas et al. (2006) who estimated eddy-fluxes of 0.3-0.4 Sv from  
214 observations at the same section. The very small eddy fluxes at the ending  
215 sections of AC and ES (Table 1) are also in agreement with Garcia-Lafuente et  
216 al (2000) and Bashek et al (2001) who found eddy-fluxes reduced to less than  
217 5% in a cross section nearby AC, and with Sanchez-Roman et al (2009) who

218 estimated similar percentages at ES. The reason why eddy fluxes are so  
 219 significant at CS and almost negligible at the ending sections of the strait is  
 220 related to the internal hydraulic of the SoG. As shown in Sannino et al. (2007)  
 221 and Sanchez-Garrido et al (2011) the hydraulic control at CS is not as  
 222 permanent as at ES or at Tarifa Narrows (Armi and Farmer., 1988), and it is  
 223 when the hydraulic control at CS is lost that eddy-fluxes participate actively in  
 224 the mean transport. As long as the hydraulic controls at ES and Tarifa Narrows  
 225 are not flooded, eddy-fluxes at AC and ES may be neglected (Vargas et al.,  
 226 2006, Sannino et al., 2007, Sanchez-Garrido et al., 2011).



227

228 Figure 2. Atlantic and Mediterranean transports versus the salinity of the isohaline  
 229 used to calculate it. Black and grey lines correspond to tidal and no-tidal runs,  
 230 respectively. Arrows indicate the maximum transport with the same color code.  
 231 Only one arrow is seen at ES because the isohaline that maximizes the transport is  
 232 the same in both runs.

233

234 Another worth noting result in Table 1 is that the exchanged flows in the non-  
 235 tidal run do not coincide with the slowly-varying contribution of the flows in the

236 tidal run (compare columns 4 and 6 in Table 1). Thus, the result of including  
 237 tides is not the mere addition of an eddy-flux contribution to the flows computed  
 238 in the non-tidal run, because this sum does not match the flows in the tidal run.  
 239 At ES and AC, the quasi-steady part of the flows in the tidal run is already  
 240 greater than the flows in the non-tidal run, but at CS, however, it is much lower.  
 241 All this highlights the complexity that tides bring to the actual exchange.

	$S_{Tid}$	$S_{No-Tid}$	$\bar{Q}_{Tid}$	$\bar{Q}_{No-Tid}$	$\Delta \%$	$\bar{u}_1 \bar{h}_1$	$\overline{u_1' h_1'}$	$\% \overline{u_1' h_1'}$
<b>ES</b>	36.6	36.6	0.988	0.935	5.7	0.957	0.031	3.0 %
<b>CS</b>	37.3	37.1	0.844	0.793	6.4	0.522	0.322	38 %
<b>AC</b>	37.5	37.3	0.893	0.823	8.5	0.880	0.013	1.4 %

242 Table 1. Computed transports (in Sv) at ES, CS and AC sections (see Fig.1). The  
 243 first two columns indicate the isohalines that maximizes the transports in each  
 244 section (see Fig.2). The third and fourth columns are the mean transport in the  
 245 tidal and non-tidal runs, respectively, and the fifth column gives the increment  
 246 (percentage) that tides cause on the transports. The term  $(\bar{u}_1 \bar{h}_1)$ , which is  
 247 representative of the slow-varying term in equation [1], is showed in the sixth  
 248 column. Eddy-fluxes  $(\overline{u_1' h_1'})$  and the percentage of the total flow that they account  
 249 for are showed in the last two columns.

250

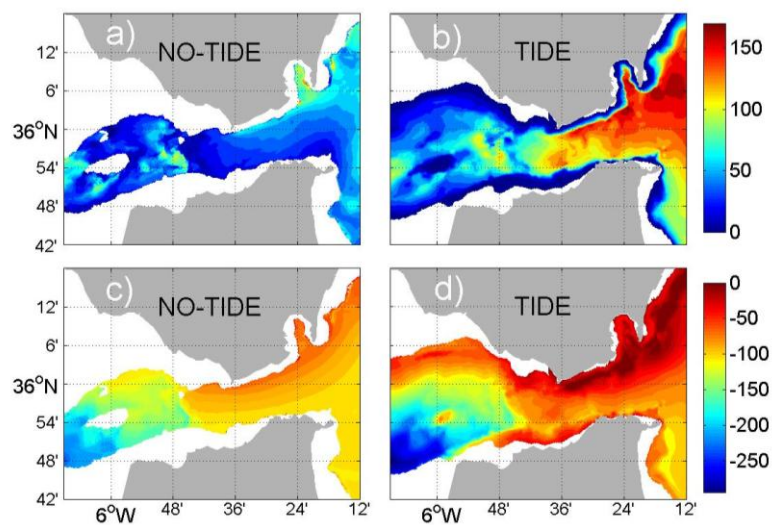
#### 251 **4.Tides modify the hydrological properties of inflowing water**

252 The most apparent local effect of tides in the SoG is the enhanced mixing  
 253 driven by shear instabilities and turbulence, whose most noticeable results are  
 254 the thickening of the interfacial layer and the modification of the hydrological  
 255 properties of their water. Both issues are addressed in this section using the  
 256 RGSM model under tidal and non-tidal runs.

257 The upper panels of Figure 3 show the interfacial layer thickness produced by  
 258 each run, calculated by fitting a hyperbolic tangent function to the vertical  
 259 salinity profiles, following Sannino et al. (2007). Lower panels indicate the depth  
 260 of the middle interface, which coincides with the inflection point of the fitted  
 261 hyperbolic tangent function. The panels show that the interfacial layer is

1 shallower in the tidal run and, consequently, covers a greater horizontal  
2 extension. Despite this increment, west of CS the thickness of the interfacial  
3 layer is much the same in both runs, but the layer becomes markedly thicker  
4 (up to 90m in certain regions) eastwards of CS in the tidal run (Figures 3a, b).  
5  
6  
7  
8  
9  
10  
11  
12  
13  
14  
15  
16  
17  
18  
19  
20  
21  
22  
23  
24  
25  
26  
27  
28  
29  
30  
31  
32  
33  
34  
35  
36  
37  
38  
39  
40  
41  
42  
43  
44  
45  
46  
47  
48  
49  
50  
51  
52  
53  
54  
55  
56  
57  
58  
59  
60  
61  
62  
63  
64  
65

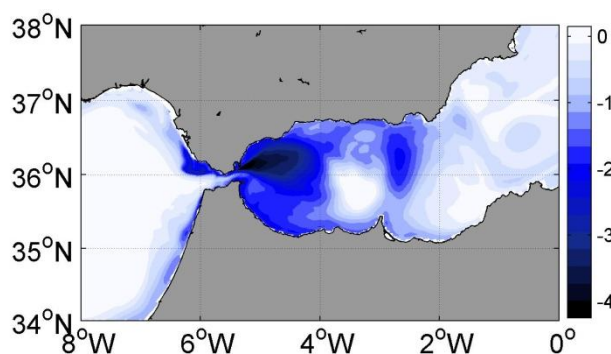
262 shallower in the tidal run and, consequently, covers a greater horizontal  
263 extension. Despite this increment, west of CS the thickness of the interfacial  
264 layer is much the same in both runs, but the layer becomes markedly thicker  
265 (up to 90m in certain regions) eastwards of CS in the tidal run (Figures 3a, b).  
266 As analyzed in Garcia-Lafuente et al. (2013), the reason for this pattern is the  
267 eastward advection of the waters that had been mixed in the Tangier basin  
268 during the previous rising tide and in the subsequent release and eastward  
269 progression of the internal hydraulic jump formed leeward of CS, which provides  
270 energy for maintaining high rates of mixing. The shoaling of the interface is  
271 primarily noticeable in north-eastern part of the Strait, where the depth of the  
272 middle interface changes from 70 m in non-tidal run to near the surface in the  
273 tidal one. The joint effect of the shoaling and thickening of the interface in the  
274 eastern half of the SoG in the tidal run is to carry water from below to the  
275 surface layers in a more effective way than in the non tidal run. In other words,  
276 AWs are expected to be saltier and colder under tidal forcing and, hence,  
277 denser and less buoyant.



278

1 279 Figure 3. a) Interface thickness, in meters, for the non-tidal run. b) Same as a) for  
2 280 the tidal run. c) Mean depth of the interface, in meters, for the non-tidal run. d)  
3 281 Same as c) for the tidal run. See text for details about the way they are computed.

4 282  
5 283 These AWs are directly advected into the adjacent Alborán Sea basin so that  
6  
7 284 the tidal run gives colder temperatures not only within the dimensions of the  
8  
9 285 SoG but also beyond its limits. Figure 4 shows the surface temperature  
10  
11 286 difference between the tidal and non-tidal simulations. The greatest differences  
12  
13 287 are found in the eastern exit of the SoG and along the expected path of the  
14  
15 288 Atlantic Jet in the western Alborán Sea, which confirms the fact that in the tidal  
16  
17 289 run the Jet carries colder water because of the enhanced tidal mixing in the  
18  
19 290 SoG. Even when reduced, this difference is still detectable in the area of the  
20  
21 291 Almería-Orán front at the eastern end of the Alborán basin and along the path  
22  
23 292 of the Algerian current further east. These visual results are confirmed by  
24  
25 293 computing the mean temperature of the incoming AWs across AC section: the  
26  
27 294 inflow is 0.37°C colder in the tidal run (15.42°C versus 15.79°C) and also 0.47  
28  
29 295 units saltier (36.63 versus 36.16). The joint effect is an inflow 0.45 kg m<sup>-3</sup>  
30  
31 296 denser in the case of the tidal run and, consequently, the flux of advected  
32  
33 297 buoyancy into the Alborán Sea diminishes. For instance, the advected  
34  
35 298 buoyancy within the 100 upper meters of the water column, computed at the AC  
36  
37 299 section, is 1.13 times lower in the tidal run (2.505 cms<sup>-2</sup> versus 2.235 ms<sup>-2</sup>),  
38  
39 300 which may have far-field significant consequences, as the cold and salty  
40  
41 301 signature generated in the SoG is exported by the Algerian current to the  
42  
43 302 interior of the MS.  
44  
45  
46  
47  
48  
49  
50  
51  
52  
53  
54  
55  
56  
57  
58  
59  
60  
61  
62  
63  
64  
65



303

304 Figure 4. Surface temperature difference ( $\theta_{tides} - \theta_{no-tides}$  in  $^{\circ}\text{C}$ ) between the tidal and  
 305 non-tidal run in the Alborán Sea.

306

### 307 **5. Tides favour Mediterranean deep water ventilation through the SoG**

308 The GSM model outputs are examined in this section to address the influence  
 309 of tides on the draining of the WMDW toward the Atlantic Ocean through the  
 310 shallow SoG. Prior to investigating the topic, it is convenient to check the model  
 311 performance, which can be assessed from Figure 5. The left panel shows the  
 312 mean temperature and salinity in the AC section (see Fig.1) provided by the  
 313 model, whereas panel b) presents observations collected in a nearby cross  
 314 section. The hydrological properties of the modelled water masses as well as  
 315 their spatial distribution match remarkably well the observations, particularly in  
 316 the lower layer, which supports the use of the GSM model to accomplish the  
 317 study of the WMDW drainage.

318 The influence of tides is assessed by comparing the volume of WMDW flowing  
 319 across the AC section computed for the tidal and non-tidal runs. In the present  
 320 study, water colder than  $13^{\circ}\text{C}$  (potential temperature) in the SoG area is  
 321 considered as WMDW. This criterion, which has been traditionally assumed in  
 322 the literature (Bryden and Stommel, 1982; Kinder and Parrilla, 1987; Kinder and  
 323 Bryden, 1990; Garcia-Lafuente et al., 2007, 2009; Naranjo et al., 2012), is

1  
2  
3  
4  
5  
6  
7  
8  
9  
10  
11  
12  
13  
14  
15  
16  
17  
18  
19  
20  
21  
22  
23  
24  
25  
26  
27  
28  
29  
30  
31  
32  
33  
34  
35  
36  
37  
38  
39  
40  
41  
42  
43  
44  
45  
46  
47  
48  
49  
50  
51  
52  
53  
54  
55  
56  
57  
58  
59  
60  
61  
62  
63  
64  
65

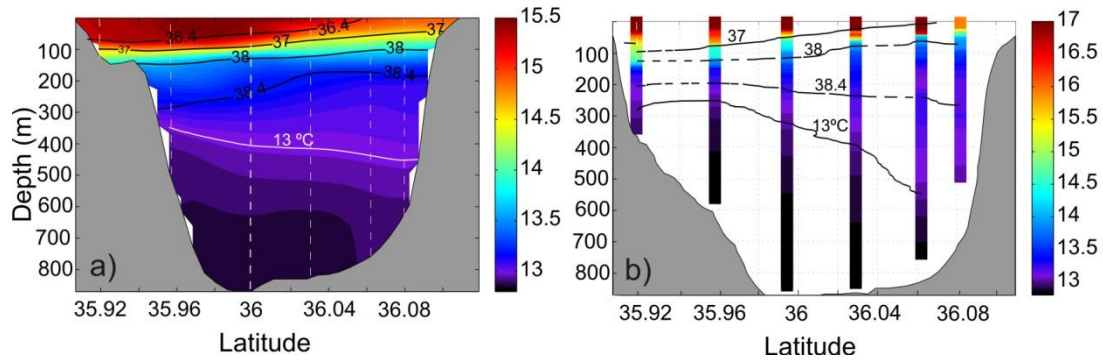
1  
2  
3  
4  
5  
6  
7  
8  
9  
10  
11  
12  
13  
14  
15  
16  
17  
18  
19  
20  
21  
22  
23  
24  
25  
26  
27  
28  
29  
30  
31  
32  
33  
34  
35  
36  
37  
38  
39  
40  
41  
42  
43  
44  
45  
46  
47  
48  
49  
50  
51  
52  
53  
54  
55  
56  
57  
58  
59  
60  
61  
62  
63  
64  
65

324 convenient in this case because the isotherm  $\theta=13$  °C is sufficiently far from the  
325 bottom in both the model and the observations (see Fig. 5) to ensure that it  
326 always lies well outside of the bottom boundary layer. Therefore, the estimated  
327 flows of WMDW are not critically dependent on the physics of the bottom  
328 boundary layer, which is not as well resolved as the ocean interior in the  
329 numerical models. Consequently, this weakness is not a major concern for our  
330 results.

331 Table 2 shows the estimated WMDW flow across AC section using the five last  
332 years of the GSM hindcast. Results for the whole 5-year period along with the  
333 values for each single year are presented in Table 2. The 5-year average is  
334 28% (0.051Sv) higher in the tidal run, although the percentage fluctuates  
335 between 10% and 50% depending on the year. The relevant result regarding  
336 this study is the visible enhancement of the WMDW aspiration in the tidal run,  
337 but the high year-to-year variability during the simulated period, which we  
338 ascribe to the internal variability of the MS and of the WMDW formation  
339 processes should also be noted.

340 A similar procedure has been carried out to estimate the WMDW flow through  
341 section WA at 3°W in the Alborán Sea (see Fig.1). Although the overall  
342 estimates point at a slight increase of WMDW volume transport toward the SoG  
343 in the tidal run, the analysis is not statistically conclusive. The fact that the  
344 comparison of tidal and non-tidal runs does not clearly detect the effect of tides  
345 on the WMDW flow through this section, located around 200 km to the east of  
346 the SoG, is interpreted as the weakening with the distance of the direct suction  
347 by tides.

348



349

350 Figure 5. a) Mean potential temperature and salinity in section AC (see Fig.1)  
 351 derived from the GSM model outputs. The filled colour contours are potential  
 352 temperature (colour bar on the right), while the labelled black contours show the  
 353 salinity. The white contour is the isotherm  $\theta=13^{\circ}\text{C}$  used as the upper limit of  
 354 WMDW (see text). b) CTD profiles collected at the -nearly- same section as in  
 355 panel a). The colour bar is again for temperature, the dashed black contours are  
 356 salinity, and the solid black line is the isotherm  $\theta=13^{\circ}\text{C}$ .

357

Block 1: $\theta < 13^{\circ}\text{C}$			
Period	$Q_{TID}(\text{Sv})$	$Q_{NOT}(\text{Sv})$	$\Delta Q(\text{Sv})/\%$
(1963-1968)	0.233	0.182	0.051 / 28
1963	0.091	0.060	0.031 / 51
1964	0.285	0.236	0.049 / 21
1965	0.307	0.230	0.077 / 33
1966	0.334	0.303	0.031 / 10
1967	0.211	0.158	0.052 / 33

358 Table 2. Time-averaged outflow of water with  $\theta < 13^{\circ}\text{C}$  across the AC section (see  
 359 Fig.1), which is identified with WMDW in this study. The first row is the five-year  
 360 average and the rest rows indicate the year-averaged WMDW outflow. Transport  
 361 with and without tides are showed in the first two columns. Last column gives the  
 362 increment between tidal and non-tidal run ( $\Delta Q$ ) and its percentage (%).

363

## 364 6. Basin scale processes, WMDW formation

365 Deep convection that leads to the formation of WMDW in the north-western MS  
 366 is among the most relevant oceanographic processes taking place in this Sea  
 367 and, as such, it has been extensively discussed in the literature (MEDOC group  
 368 1970; Schott et al., 1996; Herrmann et al., 2008; Gascard et al., 1991; Smith et  
 369 al, 2008; Marshall and Schott, 1999). The whole convection process involves

1  
2  
3  
4  
5  
6  
7  
8  
9  
10  
11  
12  
13  
14  
15  
16  
17  
18  
19  
20  
21  
22  
23  
24  
25  
26  
27  
28  
29  
30  
31  
32  
33  
34  
35  
36  
37  
38  
39  
40  
41  
42  
43  
44  
45  
46  
47  
48  
49  
50  
51  
52  
53  
54  
55  
56  
57  
58  
59  
60  
61  
62  
63  
64  
65

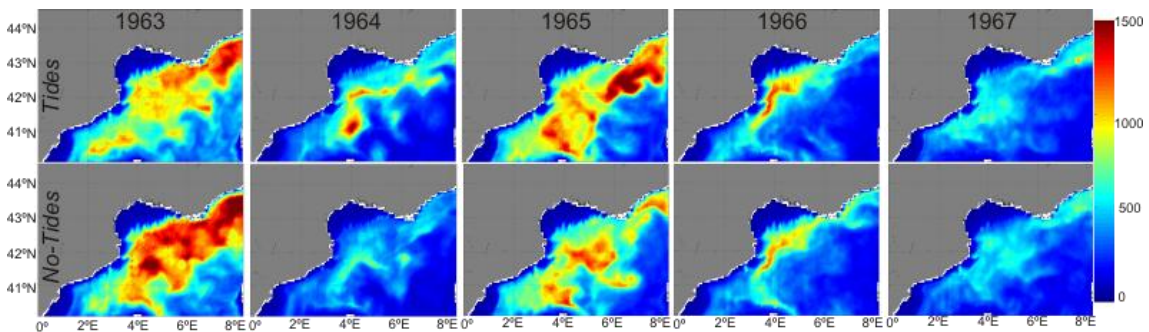
1  
2  
3  
4  
5  
6  
7  
8  
9  
10  
11  
12  
13  
14  
15  
16  
17  
18  
19  
20  
21  
22  
23  
24  
25  
26  
27  
28  
29  
30  
31  
32  
33  
34  
35  
36  
37  
38  
39  
40  
41  
42  
43  
44  
45  
46  
47  
48  
49  
50  
51  
52  
53  
54  
55  
56  
57  
58  
59  
60  
61  
62  
63  
64  
65

370 several phases. The first one is the preconditioning phase (Gascard & Richez,  
371 1985; MEDOC Group, 1970), which comprises the densification processes  
372 (buoyancy losses) that the Atlantic surface water undergoes since it enters the  
373 MS through the SoG until it sinks in winter during the second phase of the  
374 convection process. Section 4 of this study has shown that the AW inflow is  
375 colder and saltier, i.e., less buoyant, when tides are included in the model and  
376 that those signatures are carried eastwards by the Algerian current (Fig. 4). In  
377 other words, the AW in the tidal run is more strongly preconditioned than in the  
378 non-tidal run.

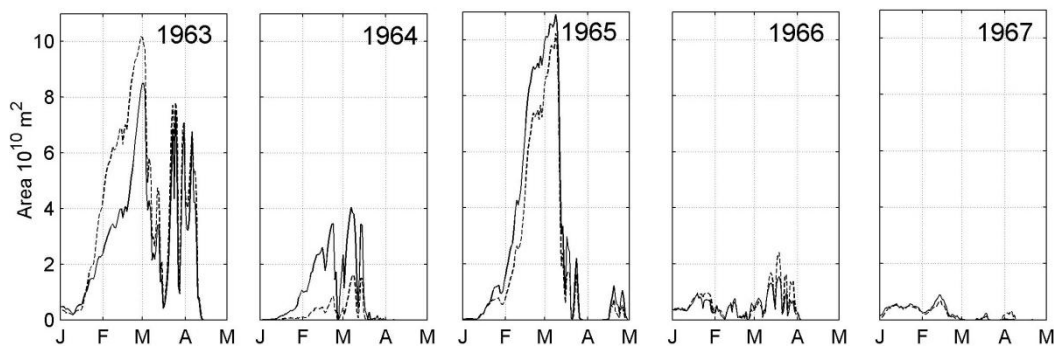
379 This section investigates whether or not this difference at the source point  
380 (SoG) has far field influence on the formation of WMDW in the Gulf of Lion area  
381 (Fig.1). The outputs of the GSM model run with and without tides are  
382 compared to address the issue. Two bulk variables or proxies are herein  
383 analyzed: the mixed layer depth (MLD) and the surface area susceptible to  
384 participate in the deep convection event (hereinafter DCA). The MLD at each  
385 grid point has been defined as the distance from the surface to the depth where  
386 the vertical diffusion coefficient reaches a threshold value of  $0.04 \text{ m}^2\text{s}^{-1}$ ,  
387 following Herrmann et al. (2008). DCA has been estimated as the area where  
388 the surface water is denser than  $1029.10 \text{ kgm}^{-3}$ , a criterion widely used in the  
389 literature of deep convection (Schott, et al., 1996; Smith, et al., 2008; Pinardi, et  
390 al. 2013).

391 Figure 6 shows the MLD averaged from January to the end of April for every  
392 year from 1963 to 1967. Maximum mean MLD reaches 1500 m during 1963,  
393 1964 and 1965, values that are quite similar to those presented by Schott et al.  
394 (1996) and Hermann et al. (2008) in the same area. Except for 1963 MLD in

395 tidal run is always greater than in non-tidal run, which is expected if tidal runs  
 396 better preconditions the inflowing AW. Figure 7 presents the evolution of the  
 397 estimated DCA during the winter months (January to end of April). The greatest  
 398 DCA is reached in March 1965 (almost  $10 \times 10^{10} \text{m}^2$  in the tidal run,  $2 \times 10^{10} \text{m}^2$   
 399 more than in non-tidal run) followed by year 1963; during this year, the DCA is  
 400 larger in the non-tidal run as it happened to the MLD too. During the rest of the  
 401 years, however, the tidal run provides larger DCA than the non tidal run. A deep  
 402 water formation rate has been calculated following Lascaratos et al. (1998) and  
 403 is presented in Figure 8a. Since it combines the former MLD and DCA  
 404 variables, the comparison of tidal and non-tidal runs does not shed new results  
 405 but confirms the previous ones, the non tidal run gives higher formation rates in  
 406 year 1963 and lower rates in all the other years.



407  
 408 Figure 6. Mixed Layer Depth in meters (colour bar) in the Gulf of Lion area (see Fig.1)  
 409 computed using a threshold value for the vertical diffusion coefficient of  $0.04 \text{m}^2 \text{s}^{-2}$ . Upper and  
 410 lower rows correspond to tidal and non-tidal runs, respectively. The contours represent the  
 411 January-to-April (both included) average.



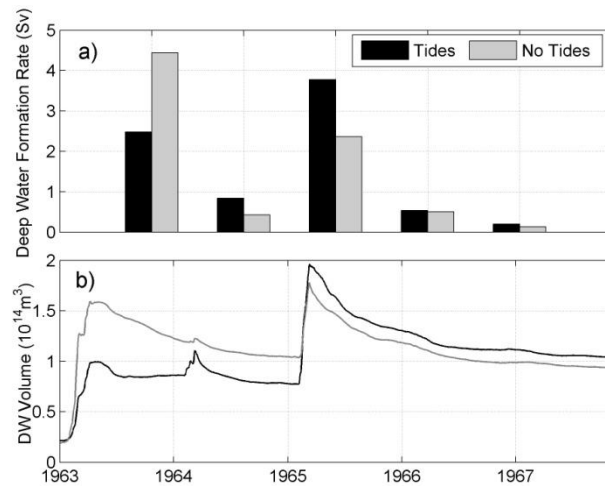
412

1 413 Figure 7. Time evolution of the Deep Convection Area in the Gulf of Lion (see Fig.1) from  
2 414 January to the end of April of every year. Solid and dashed lines represent the tidal and no-tidal  
3 415 runs respectively.

4 416  
5 417 The results presented in Figures 6 and 7 deserve some comentaries despite the  
6  
7  
8 418 topic not being the scope of this work. Focussing on the tidal run, the model  
9  
10 419 simulations predict a great year-to-year variability in all variables, namely MLD,  
11  
12 420 DCA and rate of formation. Notice the reduced DCA in years 1966 and 1967,  
13  
14 421 which is in agreement with the also diminished MLD during these years shown  
15  
16 422 in Figure 6, which in turn gives the minimum formation rate of hardly 0.2 Sv in  
17  
18 423 1967 (Fig. 8a). On the opposite end is 1965 when the rate of formation  
19  
20 424 approaches 4 Sv, a rather high value that would correspond to an exceptionally  
21  
22 425 productive year. In any case, they fall inside the interval of deep water formation  
23  
24 426 rates reported by other authors that ranges between 0.3 and 6 Sv. (Tziperman  
25  
26 427 et al., 1994, Krahnann., 1997, Castellari et al., 2000, Hermann et al., 2008,  
27  
28 428 Beranger et al., 2009, Beauvieur et al., 2012, Pinardi et al., 2013, Schott et al.,  
29  
30 429 1994 and 1996, Send et al., 1995, Schroeder et al., 2008, Durrieu de Madron et  
31  
32 430 al., 2013).

33  
34 431 Figure 8b gives the time evolution of the estimated volume of deep water  
35  
36 432 resident in the region of the Gulf of Lion as a function of time. The large  
37  
38 433 formation rate in 1963 filled up the bottom layer, which started draining out once  
39  
40 434 the winter formation processes had finished. The way it did is different for the  
41  
42 435 tidal run, in which the volume diminution stopped after a very short time of  
43  
44 436 drainage to keep constant thereafter, and the non-tidal run that featured the  
45  
46 437 exponential-like decay expected in this kind of physical problems, where the  
47  
48 438 rate of evacuation must be proportional to the volume of water that is being  
49  
50 439 evacuated. Notice that, after this year, the drainage after the refilling of the  
51  
52  
53  
54  
55  
56  
57  
58  
59  
60  
61  
62  
63  
64  
65

440 basin predicted in the tidal run shapes an exponential curve reasonably well.  
 441 We lack of a suitable explanation for the anomalous drainage in 1963, which  
 442 could be the reason explaining the apparent paradox (according to our  
 443 hypothesis) of why the non-tidal run predicts a higher rate of formation this year  
 444 than the tidal run. The footprint of the winter of 1964 is the small cusp, more  
 445 visible in the tidal run, while 1966 and 1967 with such small rates of deep water  
 446 formation, hardly leave any signal in the curve. In contrast, 1965 doubled the  
 447 volume of deep water stored in the Gulf of Lion due to the extraordinary rate of  
 448 formation, much greater in the tidal run as seen in Figure 8a.



450  
 451 Figure 8. a) Deep Water formation rate (in Sv) calculated as  $(V_A - V_B)/T$ , where  $V_A$  is  
 452 the maximum volume in a particular year,  $V_B$  is the minimum volume before the  
 453 convection event and  $T=1 \text{ year}=3.15 \cdot 10^7 \text{ s}$  (Lascaratos et al., 1998). b) Deep Water  
 454 volume measured in the volume control (Fig. 1). Black and grey colours correspond  
 455 to tidal and non-tidal run, respectively.

456  
 457 **7. Discussion and Conclusion**

458 This work examines the effect of tides in the SoG on several oceanographic  
 459 processes whose spatial scale ranges from local to basin-wide. The most  
 460 significant outcome is their contribution to increase the mean exchange that is

1  
2  
3  
4  
5  
6  
7  
8  
9  
10  
11  
12  
13  
14  
15  
16  
17  
18  
19  
20  
21  
22  
23  
24  
25  
26  
27  
28  
29  
30  
31  
32  
33  
34  
35  
36  
37  
38  
39  
40  
41  
42  
43  
44  
45  
46  
47  
48  
49  
50  
51  
52  
53  
54  
55  
56  
57  
58  
59  
60  
61  
62  
63  
64  
65

461 described here, but there are other effects intuitively related to tidal forcing that  
462 have not been thoroughly addressed to our knowledge yet. Some of them are  
463 investigated in the different sections of this work by comparing the outputs of  
464 two numerical models which have been run with and without tidal forcing.

465 As expected, the model outputs confirm that the inclusion of tides generate  
466 eddy fluxes that increase the long-term exchange. Despite its very similar  
467 contribution in the different sections of the SoG (6-8 %, see Table 1), the way  
468 the increment is achieved differs between sections. At the main CS section,  
469 eddy fluxes play a key role and represent a fundamental process to increase  
470 the long-term exchange, a result that agrees with previous findings (Bryden et  
471 al., 1994, Vargas et al., 2006). At the boundary sections of AC and ES the  
472 contribution of eddy fluxes is very small although the increment of the long-term  
473 flow due to tides is similar or even higher than at CS (8.5% at AC versus 6.4%  
474 at CS, see Table 1). A remarkable result that stems from the smallness of the  
475 eddy fluxes at the boundary sections is that the flows could be estimated  
476 satisfactorily there using only the slowly-varying term in equation [1]. It is an  
477 interesting outcome for experimental studies because the computation of eddy  
478 fluxes from observations poses serious challenges. Actually, some experimental  
479 works (Sanchez-Roman et al., 2009, Garcia-Lafuente et al. 2000) have made  
480 already use of this flow property.

481 A second effect of the tides is the enhancement of the mixing between  
482 Mediterranean and Atlantic waters within the strait itself. The energy for mixing  
483 is mainly released in the various supercritical-to-subcritical flow transitions  
484 occurring in the Tangier basin (Sanchez-Garrido et al., 2011). The final outcome  
485 is the thickening and shoaling of the interface layer in the SoG, which is favored

1  
2  
3  
4  
5  
6  
7  
8  
9  
10  
11  
12  
13  
14  
15  
16  
17  
18  
19  
20  
21  
22  
23  
24  
25  
26  
27  
28  
29  
30  
31  
32  
33  
34  
35  
36  
37  
38  
39  
40  
41  
42  
43  
44  
45  
46  
47  
48  
49  
50  
51  
52  
53  
54  
55  
56  
57  
58  
59  
60  
61  
62  
63  
64  
65

486 by the propagation of nonlinear internal waves and entrainment of MW by the  
487 Atlantic jet, an issue that has been recently addressed in Garcia-Lafuente et al.,  
488 (2013). These processes are nearly inhibited in the absence of tides, a fact that  
489 is reflected by the very thin interfacial mixing layer in the non-tidal simulation  
490 (Fig. 3). In addition to the significant effect that the shoaling of the interface may  
491 have on biological communities, the tidally-induced mixing also makes the  
492 Atlantic jet be saltier (0.47 units) and colder (0.37°C). This water is finally  
493 advected to the Alborán Sea which therefore shows colder surface waters  
494 almost everywhere although it is more visible along the mean path of the  
495 Atlantic jet and, particularly in the exit of the SoG (Figure 4). As shown recently  
496 by Sanchez-Garrido et al. (2013), the 4 °C colder surface water in this area  
497 obtained in the tidal simulation has its origin possibly in the advection of positive  
498 shear vorticity generated by the interaction of tidal currents with the solid  
499 northern boundary of the SoG. If so, this signature would be more related to the  
500 local doming of isotherms associated with the enhancement of the cyclonic  
501 circulation rather than to the direct advection of colder water from the strait. The  
502 downstream temperature anomaly in the Alborán Sea would be a consequence  
503 of this process, at least partially, but it does not modify its tidal origin.  
504 Of particular interest is the fact that the cold signature is still clearly visible in the  
505 Almería-Orán front and Algerian current, at the eastern exit of the Alborán Sea  
506 (dark blue strip over this area in Figure 4). We hypothesize that the denser AW  
507 produced by mixing in the SoG in the tidal run facilitates the formation of  
508 WMDW in the Gulf of Lion. The comparison of two bulk variables, namely MLD  
509 and DCA, suggests that indeed, the tidal run tends to produce more volume of

1  
2  
3  
4  
5  
6  
7  
8  
9  
10  
11  
12  
13  
14  
15  
16  
17  
18  
19  
20  
21  
22  
23  
24  
25  
26  
27  
28  
29  
30  
31  
32  
33  
34  
35  
36  
37  
38  
39  
40  
41  
42  
43  
44  
45  
46  
47  
48  
49  
50  
51  
52  
53  
54  
55  
56  
57  
58  
59  
60  
61  
62  
63  
64  
65

510 WMDW. However the first year of the hindcast does not behave so, as the non-  
511 tidal run produced more volume of WMDW (Figure 8).  
512 As mentioned in section 6, we lack an explanation for this behaviour, which is  
513 further puzzled by the fact that this is the only year when the drainage of the  
514 WMDW out of the control volume in the tidal run does not follow an expectable  
515 exponential decay with time (Figure 7b).  
516 Therefore, the results concerning 1963 must be interpreted cautiously. What  
517 both models predict in a similar way is the marked year-to-year variability driven  
518 by the atmospheric forcing, a variability that has also been found in other  
519 studies (Hermann et al., 2008, Pinardi et al., 2013).  
520 The last issue addressed of whether or not tides favor the ventilation of the  
521 deep WMDW layer has a positive answer according to our results. Table 2  
522 indicates that the outflow of WMDW (defined as the water colder than  $\theta=13^{\circ}\text{C}$  in  
523 the neighborhood of the SoG) increases by nearly 30% in the tidal run. This  
524 percentage is greater than the 6-7% increment of the long-term outflow due to  
525 tides (column 5 in Table 1). The difference in of percentages suggests that the  
526 drainage of WMDW is specially aided by tides and, anyway, it is more favored  
527 than any of the other Mediterranean waters participating in the outflow. Table 2  
528 also shows an interannual variability that is apparently related to the variability  
529 of the WMDW reservoir in the Gulf of Lion revealed in Figure 8. For instance,  
530 the outflow of WMDW reaches its maximum in 1966, a year after the large  
531 WMDW formation occurred in 1965. Taking into account the time the signal will  
532 take to travel from the Gulf of Lion to the SoG, this delay seems reasonable  
533 (Garcia-Lafuente et al., 2007, 2009). The trend of the WMDW stored in the  
534 control volume in the Gulf of Lion is to diminish after year 1965 (Figure 7a), a

1  
2 535 trend that seems to be followed by the outflow of WMDW with a year delay  
3 536 (Table 2).

4 537 In conclusion, our study has provided evidences that tides in the SoG has local  
5  
6 538 (increase of the long-term exchange, noticeable tidally-driven mixing, eventually  
7  
8 539 exported to the MS), regional or short-range (colder and saltier inflow,  
9  
10 540 enhanced aspiration of WMDW) and long-range (influence in deep convection  
11  
12 541 processes) influences. Of all them, the last one is more open to debate because  
13  
14 542 a convincing conclusion requires much longer simulations that include tides in  
15  
16 543 the forcing terms, which are computationally unaffordable at this moment.  
17  
18  
19  
20  
21

22 544

23  
24 545 **Acknowledgments :**

25  
26 546 This work is a contribution to the Spanish funded National Project INGRES 3  
27  
28 547 (CTM2010-21229-C02) with partially financial support of Project P08-RNM-3738  
29  
30 548 from *Plan Andaluz de Investigación*. Cristina Naranjo acknowledges the  
31  
32 549 fellowship BES-2011-043421 from the Spanish *Ministry of Economy and*  
33  
34 550 *Competitiveness*. The Mediterranean tidal simulation has been carried out thanks  
35  
36 551 to a CINECA ISCRA grant. Authors are also grateful to the Supercomputing and  
37  
38 552 Bioinformatics (SCBI) Center of the University of Malaga and to CRESCO  
39  
40 553 Supercomputing Facilities at ENEA ([www.cresco.enea.it](http://www.cresco.enea.it)).  
41  
42  
43  
44  
45  
46  
47  
48  
49  
50  
51  
52  
53  
54  
55  
56  
57  
58  
59  
60  
61  
62  
63  
64  
65

## References:

1  
2 Armi, L. and D. Farmer, 1985. The internal hydraulics of the Strait of Gibraltar  
3  
4 and associated sills and narrows. *Oceanol. Acta*, 8, 37-46.  
5  
6

7  
8  
9 Armi, L., and Farmer, D. M., 1986. Maximal two-layer exchange through a  
10  
11 contraction with barotropic net flow. *J. Fluid Mech.*, 164, 27-51.  
12  
13  
14

15  
16 Artale, V., S. Calmanti, A. Carillo, A. Dell'Aquila, M. Herrmann, G. Pisacane, P.  
17  
18 M. Ruti, G. Sannino, M.V. Struglia, F. Giorgi, X. Bi, J.S. Pal, S. Rauscher, The  
19  
20 PROTHEUS Group, 2009. An atmosphere-ocean regional climate model for  
21  
22 the Mediterranean area: assessment of a present climate simulation.  
23  
24  
25  
26 *Clim. Dyn.*, 35, 721-740, doi:10.1007/s00382-009-0691-8.  
27  
28

29  
30 Baschek, B., U. Send, J. Garcia-Lafuente, and J. Candela, 2001. Transport  
31  
32 estimates in the Strait of Gibraltar with a tidal inverse model.  
33  
34  
35  
36 *J. Geophys. Res.*, 106(C12), 31033–31044, doi:10.1029/2000JC000458.  
37  
38  
39

40  
41 Béranger, K., P. Testor, and M. Crépon, 2009. Modelling water mass formation  
42  
43 in the Gulf of Lion (Mediterranean Sea). In *Dynamics of Mediterranean Deep*  
44  
45 *Waters*, CIESM Workshop Monogr., vol. 38, edited by F. Briand,  
46  
47 pp. 91–100, Mediterr. Sci. Comm., Monaco.  
48  
49  
50

51  
52  
53 Beuvier, J., K. Béranger, C. Lebeaupin-Brossier, S. Somot, F. Sevault, Y.  
54  
55  
56 Drillet, R. Bourdallé-Badie, N. Ferry, and F. Lyard, 2012. Spreading of the  
57  
58  
59  
60  
61  
62  
63  
64  
65

1 Western Mediterranean Deep Water after winter 2005: Time scales and deep  
2 cyclone transport. *J. Geophys. Res.*, 117, C07022, doi:10.1029/2011JC007679.  
3

4  
5  
6  
7 Bray, N. A., Ochoa, J., and Kinder, T. H., 1995. The role of the interface in  
8 exchange through the Strait of Gibraltar. *J. Geophys. Res.*, 100(C6), 10755-  
9 10776, doi:10.1029/95JC00381.  
10  
11  
12

13  
14  
15  
16  
17 Bryden, H. L., and Stommel, H. M., 1982. Origin of the Mediterranean outflow.  
18  
19 *J. Mar. Res.*, 40, 55-71.  
20  
21

22  
23  
24 Bryden, H. L., and Kinder, T. H., 1991. Steady two-layer exchange through the  
25 Strait of Gibraltar. *Deep Sea Res. Part A.*, 38, S445-S463,  
26  
27 doi: 10.1016/S0198-0149(12)80020-3  
28  
29  
30

31  
32  
33  
34 Bryden, H. L., Candela, J., and Kinder, T. H., 1994. Exchange through the Strait  
35 of Gibraltar. *Prog. in Oceanog.*, 33, 201-248, doi:10.1016/0079-6611(94)90028-  
36  
37 0.  
38  
39  
40

41  
42  
43 Carrère, L., and Lyard, F., 2003. Modeling the barotropic response of the global  
44 ocean to atmospheric wind and pressure forcing-comparisons with  
45 observations. *Geophys. Res. Lett.*, 30, 1275, doi: 10.1029/2002GL016473.  
46  
47  
48  
49  
50

51  
52  
53 Castellari, S., N. Pinardi, and K. Leaman, 2000. Simulation of the water mass  
54 formation processes in the Mediterranean Sea: Influence of the time frequency  
55  
56  
57  
58  
59  
60  
61  
62  
63  
64  
65

1  
2  
3  
4  
5  
6  
7  
8  
9  
10  
11  
12  
13  
14  
15  
16  
17  
18  
19  
20  
21  
22  
23  
24  
25  
26  
27  
28  
29  
30  
31  
32  
33  
34  
35  
36  
37  
38  
39  
40  
41  
42  
43  
44  
45  
46  
47  
48  
49  
50  
51  
52  
53  
54  
55  
56  
57  
58  
59  
60  
61  
62  
63  
64  
65

of the atmospheric forcing. *J. Geophys. Res.*, 105(C10), 24,157–24,181,  
doi:10.1029/2000JC900055.

Durrieu de Madron X., L. Houpert, P. Puig, A. Sanchez-Vidal, P. Testor, A.  
Bosse, C. Estournel, S. Somot, F. Bourrin, M. N. Bouin, M. Beauverger, L.  
Beguery, A. Calafat, M. Canals, C. Cassou, L. Coppola, D. Dausse, F.  
D'Ortenzio, J. Font, S. Heussner, S. Kunesch, D. Lefevre, H. Le Goff, J. Martín,  
L. Mortier, A. Palanques and P. Raimbault, 2013. Interaction of dense shelf  
water cascading and open-sea convection in the northwestern Mediterranean  
during winter 2012. *Geophys. Res. Lett.*, 40, 1379–1385, doi:10.1002/grl.50331.

Farmer, D. M. and L. Armi, 1988. The flow of Mediterranean Water through the  
Strait of Gibraltar. *Prog. in Oceanogr.*, 21(1), 1-103.

Garcia-Lafuente, J., J. M. Vargas, F. Plaza, T. Sarhan, J. Candela, B.  
Bascheck, 2000. Tide at the eastern section of the Strait of Gibraltar.  
*J. Geophys. Res.*, 105(C6), 14197-14213, doi:10.1029/2000JC900007.

Garcia-Lafuente, J., J. Delgado, J. M Vargas, M. Vargas, F. Plaza, T. Sarhan,  
2002a. Low-frequency variability of the exchanged flows through the Strait of  
Gibraltar during CANIGO. *Deep Sea Res. Part II*, 49(19), 4051-4067.  
doi: 10.1016/S0967-0645(02)00142-X

Garcia-Lafuente, J., E. Alvarez Fanjul, J. M Vargas, A. W. Ratsimandresy,  
2002b. Subinertial variability in the flow through the Strait of Gibraltar.  
*J. Geophys. Res.*, 107(C10), 3168, doi:10.1029/2001JC001104.

1  
2 Garcia-Lafuente, J., A. Sanchez Roman, G. Díaz del Río, G. Sannino, J. C  
3  
4 Sanchez-Garrido, 2007. Recent observations of seasonal variability of the  
5  
6 Mediterranean outflow in the Strait of Gibraltar. *J. Geophys. Res.*, 112, C10005,  
7  
8 doi:10.1029/2006JC003992.  
9  
10

11  
12  
13  
14 Garcia-Lafuente, J., J. Delgado, A. Sanchez-Roman, J. Soto, L. Carracedo, G.  
15  
16 Díaz-del-Río, 2009. Interannual variability of the Mediterranean outflow  
17  
18 observed in Espartel sill, western Strait of Gibraltar. *J. Geophys. Res.*, 114,  
19  
20 C10018, doi:10.1029/2009JC005496.  
21  
22  
23

24  
25  
26 Garcia-Lafuente, J., A. Sanchez-Roman, C. Naranjo, J.C. Sanchez-Garrido,  
27  
28 2011. The very first transformation of the Mediterranean outflow in the Strait of  
29  
30 Gibraltar. *J. Geophys. Res.*, 116, C07010, doi:10.1029/2011JC006967.  
31  
32  
33

34  
35  
36 Garcia-Lafuente, J., E.B. Pozas, J.C. Sanchez-Garrido, G. Sannino, S.  
37  
38 Sammartino, 2013. The interface mixing layer and the tidal dynamics at the  
39  
40 eastern part of the Strait of Gibraltar. *J. Mar. Syst.*, 117, 31-42,  
41  
42 doi:10.1016/j.jmarsys.2013.02.014.  
43  
44  
45

46  
47  
48 Gascard, J.C. and Richez, C., 1985. Water masses and circulation in the  
49  
50 western Alborán Sea and in the Straits of Gibraltar. *Progr. In Oceanog.*, 15(3),  
51  
52 157-216.  
53  
54  
55  
56  
57  
58  
59  
60  
61  
62  
63  
64  
65

1 Gascard, J. C., 1991. Open ocean convection and deep water formation  
2 revisited in the Mediterranean, Labrador, Greenland and Weddell Seas. P. 157-  
3  
4 182. In *Deep convection and deep water formation in the oceans*, ed. By P.C.  
5  
6 Chu and J.C. Gascard, Elsevier Oceanography Series, 57, Amsterdam,  
7  
8 doi:10.1016/s0422-9894(08)70066-7.  
9

10  
11  
12  
13  
14 Helfrich, K. R., 1995. Time-dependent two-layer hydraulic exchange flows.  
15  
16  
17 *J. Phys. Oceanog.*, 25(3), 359-373.  
18

19  
20  
21 Herrmann, M., S. Somot, F. Sevault, C. Estournel, and M. Déqué  
22  
23 2008. Modeling the deep convection in the northwestern Mediterranean Sea  
24  
25 using an eddy-permitting and an eddy-resolving model: Case study of winter  
26  
27 1986–1987. *J. Geophys. Res.*, 113, C04011, doi:10.1029/2006JC003991.  
28  
29  
30

31  
32  
33  
34 Kinder, T. H., and G. Parrilla, 1987. Yes, some of the Mediterranean outflow  
35  
36 does come from great depth. *J. Geophys. Res.*, 92(C3), 2901–2906.  
37  
38

39  
40  
41 Kinder, T.H., and H. Bryden, 1990. Aspiration of deep waters through straits, in  
42  
43 *The Physical Oceanography of Sea Straits*, edited by L.J. Pratt, pp. 295-319,  
44  
45 Kluwer Acad. Norwell Mass., doi: 10.1007/978-94-009-0677-8\_14.  
46  
47

48  
49  
50  
51 Krahmann, G., Saisonale und zwischenjhrliche Variabilitim westlichen  
52  
53 Mittelmeer-Analyse historischer Daten, dissertation, 168 pp., Univ. Kiel, Kiel,  
54  
55  
56  
57 Germany, 1997.  
58  
59  
60  
61  
62  
63  
64  
65

1  
2  
3  
4  
5  
6  
7  
8  
9  
10  
11  
12  
13  
14  
15  
16  
17  
18  
19  
20  
21  
22  
23  
24  
25  
26  
27  
28  
29  
30  
31  
32  
33  
34  
35  
36  
37  
38  
39  
40  
41  
42  
43  
44  
45  
46  
47  
48  
49  
50  
51  
52  
53  
54  
55  
56  
57  
58  
59  
60  
61  
62  
63  
64  
65

Lascaratós, A., and Nittis, K., 1998. A high-resolution three-dimensional numerical study of intermediate water formation in the Levantine Sea. *J. Geophys. Res.*, 103(C9), 18497-18511, doi: 10.1029/98JC01196.

Leith, C. E., 1968. Diffusion approximation for two-dimensional turbulence. *Physics of Fluids*, 11, 671, doi:10.1063/1.1691968.

Macías, D., A. P. Martín, J. García-Lafuente, C. M. García, A. Yool, M. Bruno, F. Echevarría, 2007. Analysis of mixing and biogeochemical effects induced by tides on the Atlantic–Mediterranean flow in the Strait of Gibraltar through a physical–biological coupled model. *Progr. Oceanog.*, 74(2), 252-272, doi:10.1016/j.ocean.2007.04.006.

Marshall, J., C. Hill, L. Perelman, A. Adcroft, 1997a. Hydrostatic, quasi-hydrostatic, and nonhydrostatic ocean modeling. *J. Geophys. Res.*, 102(C3), 5733–5752, doi:10.1029/96JC02776.

Marshall, J., A. Adcroft, C. Hill, L. Perelman, C. Heisey, 1997b, A finite-volume, incompressible Navier Stokes model for studies of the ocean on parallel computers. *J. Geophys. Res.*, 102, 5753–5766, doi:10.1029/96JC02775.

Marshall, J., and Schott, F., 1999. Open-ocean convection: Observations, theory, and models. *Reviews of Geophysics*, 37(1), 1-64, doi:10.1029/98RG02739.

1 MEDOC Group, Observations of formation of deep-water in the Mediterranean  
2 Sea, 1969. *Nature*, 227, 1037–1040.  
3

4  
5  
6  
7 Mikolajewicz, U., 2011, Modeling Mediterranean Ocean climate of the last  
8 glacial maximum. *Clim. Past*, 7, 161-180, doi: 10.5194/cp-7-161-2011.  
9

10  
11  
12  
13  
14 Naranjo, C., J. Garcia-Lafuente, J. C. Sanchez-Garrido, A. Sanchez-Roman, J.  
15 Delgado Cabello, 2012. The western Alborán gyre helps ventilate the western  
16 Mediterranean deep water through Gibraltar. *Deep Sea Res. Part I*, 63, 157-  
17 163, doi:10.1016/j.dsr.2011.10.003.  
18  
19  
20  
21  
22

23  
24  
25  
26 Oddo, P., M. Adani, N. Pinardi, C. Fratianni, M. Tonani, D. Pettenuzzo, 2009. A  
27 nested Atlantic-Mediterranean Sea general circulation model for operational  
28 forecasting. *Ocean Sci.* 5, 461–473, doi:10.5194/os-5-461-2009, 2009.  
29  
30  
31  
32

33  
34  
35  
36 Pacanowski, R. C., and Philander, S. G. H., 1981. Parameterization of vertical  
37 mixing in numerical models of tropical oceans. *J. Phys. Oceanog*, 11(11), 1443-  
38 1451.  
39  
40  
41  
42

43  
44  
45 Pinardi, N., M. Zavatarelli, M. Adani, G. Coppini, C. Fratianni, P. Oddo, A.  
46 Bonaduce, 2013. Mediterranean Sea large-scale low-frequency ocean  
47 variability and water mass formation rates from 1987 to 2007: a retrospective  
48 analysis. *Prog. in Oceanog*, doi:10.1016/j.pocean.2013.11.003, (in press).  
49  
50  
51  
52  
53  
54  
55  
56  
57  
58  
59  
60  
61  
62  
63  
64  
65

1 Sammartino S., J. Garcia-Lafuente, J. C. Sanchez-Garrido, F. J. De los Santos,  
2 E. ÁlvarezFanjul, C. Naranjo, M. Bruno, C. Calero, 2014. A numerical model  
3 analysis of the tidal flows in the Bay of Algeciras, Strait of Gibraltar. *Continental*  
4 *Shelf Res.*, 72, 34-46, doi:10.1016/j.csr.2013.11.002.  
5  
6  
7  
8  
9

10  
11 Sanchez-Garrido, J. C., G. Sannino, L. Liberti, J. Garcia-Lafuente, L. Pratt,  
12 2011. Numerical modeling of three-dimensional stratified tidal flow over  
13 Camarinal Sill, Strait of Gibraltar. *J. Geophys. Res.*, 116, C12026,  
14 doi:10.1029/2011JC007093.  
15  
16  
17  
18  
19  
20  
21

22  
23 Sanchez-Garrido, J. C., J. Garcia-Lafuente, E. Álvarez-Fanjul, M. Sotillo, F. J.  
24 de-los-Santos, 2013. What does cause the collapse of the Western Alborán  
25 Gyre? Results of an operational ocean model. *Prog. in Oceanog.*, 116, 142-  
26 153, doi:10.1016/j.pocean.2013.07.002 .  
27  
28  
29  
30  
31  
32

33  
34  
35 Sanchez-Román, A., G. Sannino, J. Garcia-Lafuente, A. Carillo, F.  
36 Criado-Aldeanueva, 2009. Transport estimates at the western section of the  
37 Strait of Gibraltar: A combined experimental and numerical modeling study.  
38 *J. Geophys. Res.*, 114, C06002, doi:10.1029/2008JC005023.  
39  
40  
41  
42  
43  
44  
45

46  
47 Sannino, G., A. Bargagli, V. Artale, 2004. Numerical modeling of the  
48 semidiurnal tidal exchange through the Strait of Gibraltar. *J. Geophys.*  
49 *Res*, 109, C050115, doi:10.1029/2003JC002057.  
50  
51  
52  
53  
54  
55  
56  
57  
58  
59  
60  
61  
62  
63  
64  
65

1  
2  
3  
4  
5  
6  
7  
8  
9  
10  
11  
12  
13  
14  
15  
16  
17  
18  
19  
20  
21  
22  
23  
24  
25  
26  
27  
28  
29  
30  
31  
32  
33  
34  
35  
36  
37  
38  
39  
40  
41  
42  
43  
44  
45  
46  
47  
48  
49  
50  
51  
52  
53  
54  
55  
56  
57  
58  
59  
60  
61  
62  
63  
64  
65  
Sannino, G., A. Carillo, V. Artale, 2007. Three-layer view of transports and hydraulics in the Strait of Gibraltar: A three-dimensional model study, *J. Geophys. Res.*, 112, C03010, doi:10.1029/2006JC003717.

Sannino, G., J. C. Sanchez Garrido, L. Liberti and L. Pratt, 2014 Exchange Flow through the Strait of Gibraltar as Simulated by a  $\sigma$ -Coordinate Hydrostatic Model and a z-Coordinate Nonhydrostatic Model. In *The Mediterranean Sea: Temporal Variability and Spatial Patterns* (eds G. L. E. Borzelli, M. Gačić, P. Lionello and P. Malanotte-Rizzoli), John Wiley & Sons, Inc., Oxford. doi: 10.1002/9781118847572.ch3

Schott, F., M. Visbeck, and U. Send, 1994. Open ocean deep convection, Mediterranean and Greenland Seas. In *Ocean Processes on Climate Dynamics: Global and Mediterranean Examples*, edited by P. Malanotte-Rizzoli and A. R. Robinson, pp. 203–225, Kluwer Acad., Norwell, Mass.

Schott, F., M. Visbeck, U. Send, J. Fischer, L. Stramma, Y. Desaubies, 1996. Observations of deep convection in the Gulf of Lions, northern Mediterranean, during the winter of 1991/92. *J. Phys. Oceanog.*, 26(4), 505-524, doi: 10.1175/1520-0485(1996)026<0505:OODCIT>2.0.CO;2

Schroeder, K., A. Ribotti, M. Borghini, R. Sorgente, A. Perilli, and G. P. Gasparini, 2008. An extensive western Mediterranean deep water renewal between 2004 and 2006. *Geophys. Res. Lett.*, 35, L18605, doi:10.1029/2008GL035146.

1 Send, U., F. Schott, F. Gaillard, and Y. Desaubies, 1995. Observation of a deep  
2 convection regime with acoustic tomography. *J. Geophys. Res.*, 100(C4), 6927–  
3  
4 6941, doi:10.1029/94JC03311.  
5  
6

7  
8  
9 Smith, R. O., H. L. Bryden, K. Stansfield, 2008. Observations of new western  
10 Mediterranean deep water formation using Argo floats 2004-2006. *Ocean*  
11  
12 *Science*, 4(2), 133-149.  
13  
14  
15

16  
17  
18 Stommel, H., Bryden, H., and Mangelsdorf, P., 1973. Does some of the  
19 Mediterranean outflow come from great depth? *Pure and Applied Geophysics*,  
20  
21 105(1), 879-889.  
22  
23  
24  
25

26  
27  
28 Tziperman, E., and Speer, K., 1994. A study of water mass transformation in  
29 the Mediterranean Sea: Analysis of climatological data and a simple three-box  
30  
31 model. *Dyn. Atmos. Oceans*, 21, 53–82, doi: 10.1016/0377-0265(94)90004-3  
32  
33  
34  
35

36  
37  
38 Vargas, J. M., J. Garcia-Lafuente, J. Candela, A. J. Sanchez, 2006. Fortnightly  
39 and monthly variability of the exchange through the Strait of Gibraltar. *Prog.*  
40  
41 *Oceanog.*, 70(2), 466-485. doi:10.1016/j.pocean.2006.07.001.  
42  
43  
44  
45

46  
47  
48 Vázquez, A., M. Bruno, A. Izquierdo, D. Macías, A. Ruiz-Cañavate, 2008.  
49 Meteorologically forced subinertial flows and internal wave generation at the  
50  
51 main sill of the Strait of Gibraltar. *Deep Sea Res. Part I*, 55(10), 1277-1283,  
52  
53  
54  
55  
56  
57  
58  
59  
60  
61  
62  
63  
64  
65  
doi:10.1016/j.dsr.2008.05.008.

1 Vázquez, A., S. Flecha, M. Bruno, D. Macías, G. Navarro, G., 2009. Internal  
2 waves and short-scale distribution patterns of chlorophyll in the Strait of  
3 Gibraltar and Alborán Sea. *Geophys. Res. Lett.*, 36(23), L23601,  
4 doi:10.1029/2009GL040959  
5  
6  
7  
8  
9

10 Wang, D. P., 1993. The Strait of Gibraltar Model: Internal tide, diurnal inequality  
11 and fortnightly modulation. *Deep Sea Res. Part I*, 40(6), 1187-1203,  
12 doi:10.1016/0967-0637(93)90133-N.  
13  
14  
15  
16  
17  
18  
19  
20

21 Wesson, J. C., and Gregg, M. C., 1994. Mixing at Camarinal sill in the Strait of  
22 Gibraltar. *J. Geophys. Res.: Oceans*, (1978–2012), 99(C5), 9847-9878,  
23 doi:10.1029/94JC00256.  
24  
25  
26  
27  
28  
29  
30

31 Whitehead Jr., J. A., 1985. A laboratory study of gyres and uplift near the Strait  
32 of Gibraltar, *J. Geophys. Res.*, 90(C4), 7045–7060,  
33 doi:10.1029/JC090iC04p07045.  
34  
35  
36  
37  
38  
39  
40  
41  
42  
43  
44  
45  
46  
47  
48  
49  
50  
51  
52  
53  
54  
55  
56  
57  
58  
59  
60  
61  
62  
63  
64  
65